An algorithm to prune the area-preserving Hénon map

2004 J. Phys. A: Math. Gen. 37 10521

(http://iopscience.iop.org/0305-4470/37/44/005)

INSTITUTE OF PHYSICS PUBLISHING JOURNAL OF PHYSICS A: MATHEMATICAL AND GENERAL

J. Phys. A: Math. Gen. **37** (2004) 10521–10543 PII: S0305-4470(04)78946-5

An algorithm to prune the area-preserving Hénon map

Ryouichi Hagiwara and Akira Shudo

Department of Physics, Tokyo Metropolitan University, Minami-Ohsawa, Hachioji, Tokyo 192-0397, Japan

E-mail: ryouichi@comp.metro-u.ac.jp and shudo@phys.metro-u.ac.jp

Received 7 April 2004, in final form 2 September 2004
Published 20 October 2004
Online at stacks.iop.org/JPhysA/37/10521
doi:10.1088/0305-4470/37/44/005

Abstract

An explicit algorithm to provide the pruning front for the area-preserving Hénon map is presented. The procedure terminates within finitely many steps when the map has hyperbolic structure. The only information required to specify the pruning front is a bifurcation diagram of homoclinic orbits, and it is obtained by tracking orbits from the anti-integrable limit. The pruned region thus determined is used to construct the Markov partition of the map, and the topological entropy is evaluated as an application.

PACS numbers: 05.45.−a, 05.45.Ac

1. Introduction

A critical ingredient in the description of chaotic dynamics is the topology of the nonwandering set. The kneading theory of Milnor and Thurston provides us with a precise recipe to specify all topological natures of a family of unimodal maps [1]. The kneading sequence, which is defined as the itinerary of the critical point, gives a border between admissible and nonadmissible orbits in appropriate symbolic representation. In contrast to one-dimensional maps, it is no longer valid, except for quasi one-dimensional situations [2], to carry out an analogous programme for more than one-dimensional maps due to the lack of critical points. We have to find an alternative way to capture topological aspects of higher dimensional maps.

The idea of a *pruning front* has been proposed as a natural extension of the kneading theory; it gives an analogous border in the two-dimensional symbol plane, which also determines admissible and nonadmissible orbits [3, 4]. To explain the idea, assume a certain once-folding map with a complete horseshoe and then prepare the two-dimensional symbol plane, which is shown in figure 1(*a*). Each point of the symbol plane corresponds to a point on the nonwandering set, and has a doubly infinite symbolic representation. As the system parameter is varied, as shown in figure 1(*b*), a complete horseshoe is destroyed and a certain set of points in the symbol plane may lose the corresponding orbits in the dynamics. Some regions in the

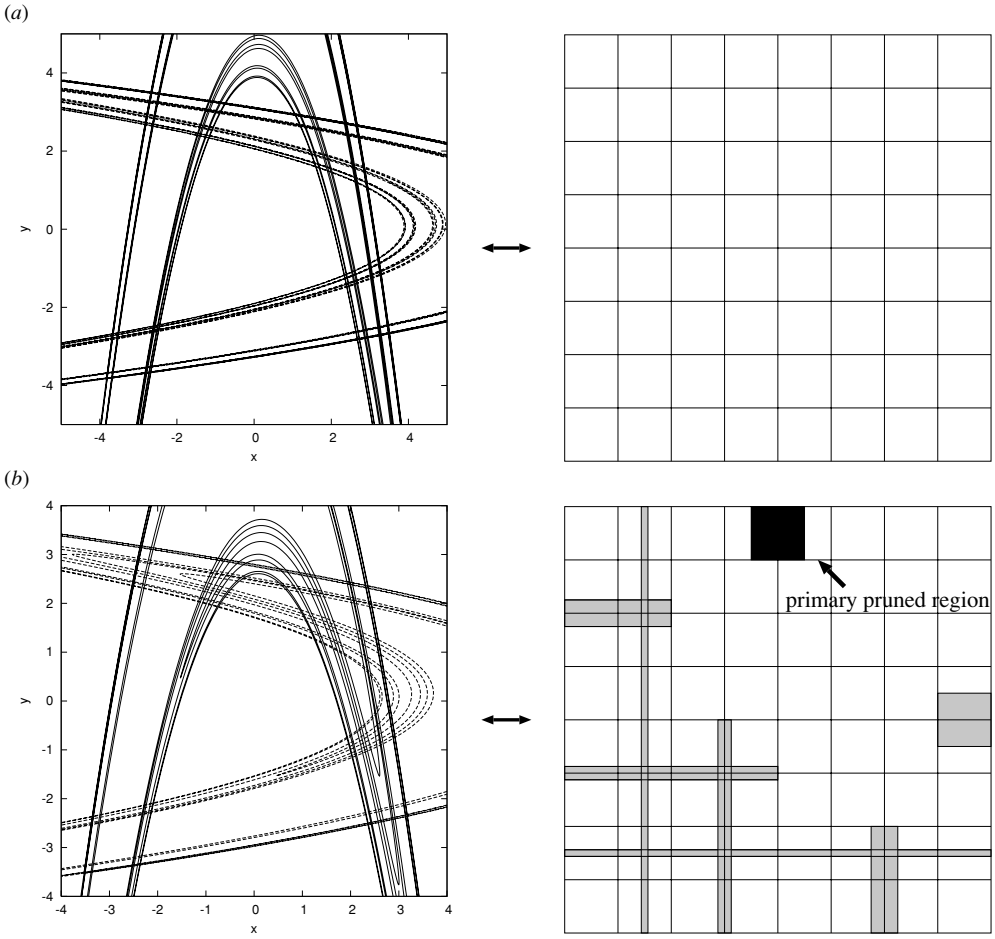

Figure 1. Examples of horseshoes for the area-preserving Hénon map and the symbol planes. (*a*) Complete horseshoe. (*b*) Incomplete horseshoe and the corresponding pruned regions shown as black and grey blocks.

symbol plane are *pruned* in this way, and the border, which divides the symbol plane into admissible and nonadmissible regions, is called the *pruning front*. Clearly, the pruning front was introduced to play a similar role to a critical point in the kneading theory.

The *pruning front conjecture* is concerned with a prediction that all forbidden orbits are specified solely by the pruning front and that there are no other independent pruning mechanisms. Although this has not been rigorously established yet, its validity was checked numerically [3, 5]. It was shown afterwards that the proposed programme is indeed realizable [6]. More precisely, the author of [6] gave a mathematical formulation of the problem and an explicit representation of the pruning front for the Lozi map [7].

Generic two-dimensional maps such as the Hénon map [8], which is classified as the simplest polynomial automorphism having non-trivial dynamics [9], are also to be studied in a similar manner, but a concrete recipe as given for the Lozi map has not been successfully presented yet. There is evidence implying that constructing a symbolic representation of the area-preserving Hénon map would be difficult in general [10]. On the other hand, a

mathematical definition of pruning fronts and the pruning theorem based on it have been presented [11, 12]. They also provided an algorithm which enables us to have a maximal pruning of the horseshoe for each given orbit, together with a computer code to realize it [13].

The purpose of our work is to give an explicit algorithm to compute the pruning front for the area-preserving Hénon map

$$H_{a,b}: \begin{pmatrix} x \\ y \end{pmatrix} \to \begin{pmatrix} a + by - x^2 \\ x \end{pmatrix}, \tag{1}$$

where $|b| = 1$. It provides the pruned region for a given parameter value at which the map has hyperbolic structure. So it differs from the algorithm presented in [13], in which for a given orbit the maximal pruned region is obtained. As explained in section 4, we use the term hyperbolicity in a little restricted sense: the situation where the stable manifold accumulates to a segment of the unstable manifold will be excluded. Since we concentrate here on the case $b = -1$, we will drop the subscript b and denote the map by H_a hereafter.

Our work is motivated by numerical finding, together with pieces of convincing evidence, that even in the non-horseshoe parameter region there exist a lot of, or presumably infinitely many, sub-intervals in which the Hénon map has hyperbolic structure [14]. Hyperbolicity of dynamics implies a Markov shift, and the authors actually constructed it in a heuristic manner [14].

It should be noted that the pruned region cannot be determined uniquely because, by definition, forward and backward iterations of some pruned region yield other pruned regions. So it may have redundancy unless additional conditions are specified. The *primary pruned region* has been proposed to avoid such ambiguity [3, 4]. Here, we define the primary pruned region as a region D satisfying the following properties:

- An orbit is admissible if and only if all of its forward and backward images lie outside D.
- The boundary of D is *monotone* in each half of the symbol plane, and is symmetric with respect to the vertical centre line.

Otherwise stated, we fix our pruned region by specifying the second condition. In figure 1(b), we present an example of the primary pruned region (shown as a black one) for the area-preserving Hénon map obtained by our algorithm.

Several attempts have been made to give the generating partition of the Hénon map by introducing the primary homoclinic tangencies [2, 15–19]. We do not intend to construct the generating partition. Instead, we assume that every homoclinic orbit keeps its own code, which is assigned in the anti-integrable limit, i.e. $a \to \infty$, until it bifurcates. What we will do is just draw the pruning front in the symbol plane under the assumption that the system possesses hyperbolic structure.

Crucial information we have to keep in advance is a bifurcation diagram of homoclinic orbits on a certain fundamental segment of the stable (or unstable) manifold. An important fact is that all combinatorial data are contained in it. Such a diagram is obtained by applying a continuation method proposed by Sterling *et al* [20, 21], which we now briefly describe. They use an approximation of a homoclinic orbit by a sequence of periodic orbits which approaches it as the period increases. Rewriting (1) as a second-order difference equation and changing its variables as $z = \epsilon x$ and $\epsilon = a^{-1/2}$ give

$$\epsilon(z_{j+1} - bz_{j-1}) + {z_j}^2 - 1 = 0. \tag{2}$$

We denote a period n orbit of (2) by $\mathbf{z}(\epsilon)$. At the anti-integrable limit $\epsilon \to 0$, the map reduces to ${z_j}^2 = 1$. Therefore an orbit is an arbitrary sequence of ± 1, which we denote

by $\mathbf{s}$. Continuation of $\mathbf{z}(\epsilon)$ is to calculate smooth curves in $\mathbb{R}^n \times \mathbb{R}$ satisfying the following conditions:

$$\mathbf{G}(\mathbf{z}, \epsilon) = \mathbf{0} \qquad \text{and} \qquad \mathbf{z}(0) = \mathbf{s},$$

where the jth component of $\mathbf{G}$ is the left-hand side of (2). Each curve extends to some parameter value at which the orbit bifurcates, and returns to the limit.

The continuation method is based on the assumption that all orbits of the map are continuously connected to the limit, $a \to \infty$. In other words, it is assumed that there are no isolated 'bubbles' in the bifurcation diagram. In the area-preserving case, this assumption is quite reasonable. According to Sterling *et al* [21, 22], even though there are exceptional orbits breaking it, the number of such orbits of low period is very small. On the other hand in the dissipative case, the map generically creates orbits when the parameter a decreases, and the topological entropy is not necessarily monotone [23]. Note that our algorithm presented in this paper cannot control such bubbles. This is a serious obstacle to apply the algorithm to dissipative maps.

The paper is organized as follows. After some preliminaries in section 2, we give our algorithm explicitly in section 3. In section 4, justification of our algorithm is presented. Then in section 5, we show several examples of pruned regions. Especially, detailed procedures are traced in one of those examples. In section 6, we give how the pruned region thus constructed can be converted into a Markov partition and the corresponding structure matrix, which allows us to compute the topological entropy of the map. Finally in section 7, we summarize the paper and discuss some open problems.

2. Preliminaries

In this section, we introduce notation and terminology for subsequent arguments and present some basic propositions employed to ensure our algorithm.

2.1. Symbolic dynamics

The area-preserving Hénon map H_a is conjugate to the horseshoe map if a is sufficiently large [24]. However, at a certain parameter value, which was numerically evaluated as $a_f = 5.699\ldots$ [25], the first homoclinic bifurcation between the innermost stable and the outermost unstable manifolds happens. This event is called the *first tangency*, and a recent work using the theory of complex dynamics rigorously proved that the Hénon map keeps the horseshoe structure until the first tangency point [26].

In the horseshoe region, an orbit in the nonwandering set Λ corresponds one-to-one to a doubly infinite sequence in the shift space $\Sigma_2 = \{0, 1\}^{\mathbf{z}}$. The dynamics on Σ is represented by the shift map, $\sigma : \Sigma \to \Sigma$, defined as $\sigma(\ldots s_{-1} \cdot s_0 s_1 \ldots) = (\ldots s_{-1} s_0 \cdot s_1 \ldots)$, where '$\cdot$' denotes the current time of the orbit. A periodic orbit of the original map corresponds to a periodic symbol sequence, $(s_0 s_1 \ldots s_{n-1})^\infty = (\ldots s_{n-1} \cdot s_0 s_1 \ldots s_{n-1} s_0 \ldots)$, and so the two fixed points of the map are $(0)^\infty$ and $(1)^\infty$. An orbit homoclinic to $(0)^\infty$ is then expressed as a symbol sequence of the form $(0^\infty 1 s_{-t} \ldots s_{-1} \cdot s_0 \ldots s_{h-1} 10^\infty)$.

For a symbol sequence $\mathbf{s} = (\ldots s_{-2} s_{-1} \cdot s_0 s_1 s_2 \ldots)$, we call $\mathbf{s}_+ := s_0 s_1 s_2 \ldots$ its *head* and $\mathbf{s}_- := \ldots s_{-2} s_{-1}$ its *tail*, and denote it in shorthand by $\mathbf{s} = (\mathbf{s}_- \cdot \mathbf{s}_+)$. The nonwandering set Λ can be identified with a unit square, which is used as the symbol plane (see figure 2). There is ambiguity because every dyadic rational point in the symbol plane corresponds to four homoclinic points. Therefore, we will sometimes use the trellis of the stable and unstable

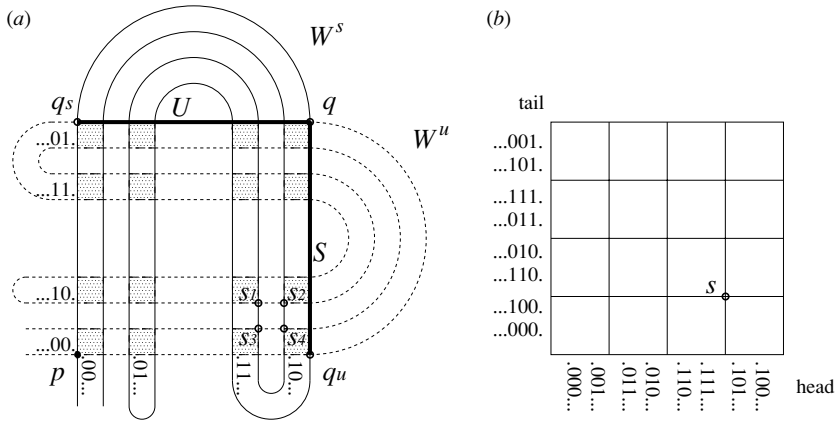

Figure 2. (*a*) Trellis of the stable and unstable manifolds. Two thick lines indicate the fundamental segments. (*b*) The symbol plane $\Sigma_2 = \{0, 1\}^{\mathbf{z}}$. Four homoclinic points $\mathbf{s}_1, \mathbf{s}_2, \mathbf{s}_3$ and $\mathbf{s}_4$ in (*a*) correspond to a single point $\mathbf{s}$ in (*b*).

manifolds, denoted by W^s and W^u respectively, to avoid confusions. Using the unimodal ordering [27], we define the ordering of heads and tails as

$$\begin{aligned} \cdot e0\ldots &\prec \cdot e1\ldots \\ \cdot o0\ldots &\succ \cdot o1\ldots \\ \ldots 0e\cdot &\prec \ldots 1e\cdot \\ \ldots 0o\cdot &\succ \ldots 1o\cdot, \end{aligned} \tag{3}$$

where the number of 1s in e (resp. o) is even (resp. odd).

2.2. Homoclinic orbits

Following the discussion developed in [21], we here focus on homoclinic orbits of the outer hyperbolic fixed point p. Even if we choose alternative fixed points or periodic points instead of p, the following argument holds in a similar way.

We denote a closed segment of W^u with endpoints q and r by $W^u[q, r]$, and an open segment by $W^u(q, r)$. The two segments, $U := W^u[q, q_s]$ and $S := W^s[q, q_u]$ in figure 2, are called the *fundamental segments* [21, 28]. Note that every homoclinic orbit has exactly one point on a segment from q_u to $q_s = H_a(q_u)$, and that there are no homoclinic points on $W^u(q_u, q)$.

The homoclinic orbits (except for q, q_s and q_u) on the fundamental segments can be expressed in the form:

$$\begin{aligned} &(0^\infty 1 \cdot s_0 s_1 \ldots s_{T-1} 10^\infty) \quad \text{on } U \\ &(0^\infty 1 s_0 s_1 \ldots s_{T-1} \cdot 10^\infty) \quad \text{on } S. \end{aligned}$$

In these sequences, T is called the *transition time* of the orbit [21], because this is the number of iterations required for a point on U to reach S. We define the transition time of q and $q_s = H_a(q_u)$ in figure 2 as 0.

As mentioned in the introduction, even after the first tangency, we assume that every homoclinic orbit keeps its own horseshoe code. An orbit undergoing a pitchfork bifurcation needs careful consideration. We here adopt a rule, which is slightly different from the one given by Sterling *et al* [21], to assign the codes to homoclinic orbits involved in a pitchfork

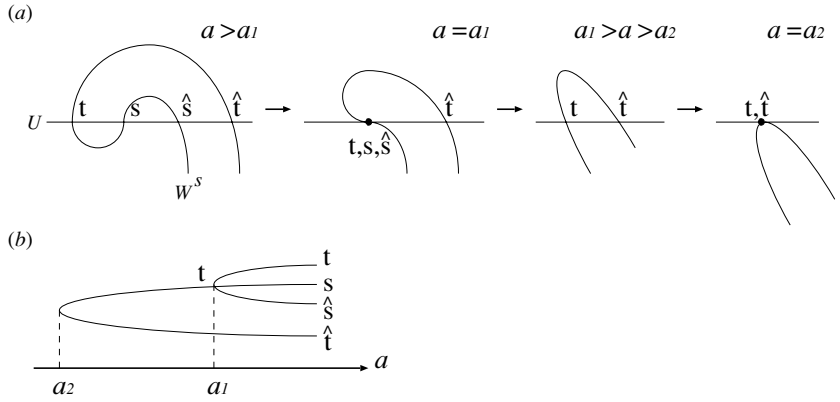

Figure 3. Pitchfork bifurcation followed by a saddle-node bifurcation. (*a*) Three points **s**, $\hat{\mathbf{s}}$ and **t** degenerate into a single point **t** at $a = a_1$, and then it collides with $\hat{\mathbf{t}}$ at $a = a_2$. Since **s** and $\hat{\mathbf{s}}$ are symmetric with respect to the vertical centre line, **t** survives after they degenerate. (*b*) The bifurcation diagram of (*a*).

bifurcation: first iterate three homoclinic points on U undergoing a pitchfork bifurcation so that the symbol sequences of the shifted points coincide in the tail part and that the discrepancy occurs at the first digit of the head part. In such a configuration, the two of them are necessarily symmetric with respect to the vertical centre line. In figure 3, the points **s** and $\hat{\mathbf{s}}$ represent the symmetric pair. We assign the symbol sequence owned by the other point **t** to the point that survives after the bifurcation. In the case of an asymmetric-type pitchfork bifurcation [21] or more higher order bifurcations, we can adopt a similar rule.

2.3. Pruned pairs

For a homoclinic point $\mathbf{s} = \left(0^\infty 1 s_{-T_t} \dots s_{-1} \cdot s_0 \dots s_{T_h-1} 10^\infty\right)$, we introduce the following notation

$$\begin{aligned} N_u(\mathbf{s}) &:= \left(0^\infty 1 s_{-T_t} \dots s_{-1} \cdot s_0 \dots s_{T_h-2} \hat{s}_{T_h-1} 10^\infty\right) \\ N_s(\mathbf{s}) &:= \left(0^\infty 1 \hat{s}_{-T_t} s_{-T_t+1} \dots s_{-1} \cdot s_0 \dots s_{T_h-1} 10^\infty\right), \end{aligned} \tag{4}$$

where $\hat{s}_j = 1 - s_j$. We show an example in figure 2, in which $\mathbf{s}_2 = N_u(\mathbf{s}_1)$ and $\mathbf{s}_3 = N_s(\mathbf{s}_1)$. The symbol N stands for 'neighbour', so if both **s** and $N_u(\mathbf{s})$ (resp. $N_s(\mathbf{s})$) exist (i.e. are not pruned yet), they are neighbouring homoclinic points on W^u (resp. W^s). That is, there are no other homoclinic points on either $W^u(\mathbf{s}, N_u(\mathbf{s}))$ or $W^s(\mathbf{s}, N_s(\mathbf{s}))$.

Similarly, for a homoclinic point $\mathbf{s} = \left(0^\infty 1 s_{-T_t} \dots s_{-1} \cdot s_0 \dots s_{T_h-1} 10^\infty\right)$, we introduce the notation

$$\begin{aligned} P_u(h, \mathbf{s}) &:= \left(0^\infty 1 s_{-T_t} \dots s_{-1} \cdot s_0 \dots s_{h-1} \hat{s}_h 0^\infty\right) && (h \geqslant T_h) \\ P_s(t, \mathbf{s}) &:= \left(0^\infty \hat{s}_{-t-1} s_{-t} \dots s_{-1} \cdot s_0 \dots s_{T_h-1} 10^\infty\right) && (t \geqslant T_t), \end{aligned} \tag{5}$$

where $s_{T_h} = s_{-T_t-1} = 1$ and $s_j = 0$ for all $j \leqslant -T_t - 2$, $T_h + 1 \leqslant j$. Roughly speaking, as shown in figure 4, **s** and $P_u(h, \mathbf{s})$ are the endpoints of a segment of $H_a^{-h}(R) \cap W^u$, where R is the whole quadrilateral bounded by W^u and W^s. The larger the subscripts h and t become, the larger the transition times of $P_u(h, \mathbf{s})$ and $P_s(t, \mathbf{s})$ become and the closer they approach **s**. Particularly on U, h is equal to the transition time of $P_u(h, \mathbf{s})$ except for the case $h = T_h$ (see (5)). Similarly on S, t is the transition time of $P_s(t, \mathbf{s})$ except for $t = T_t$.

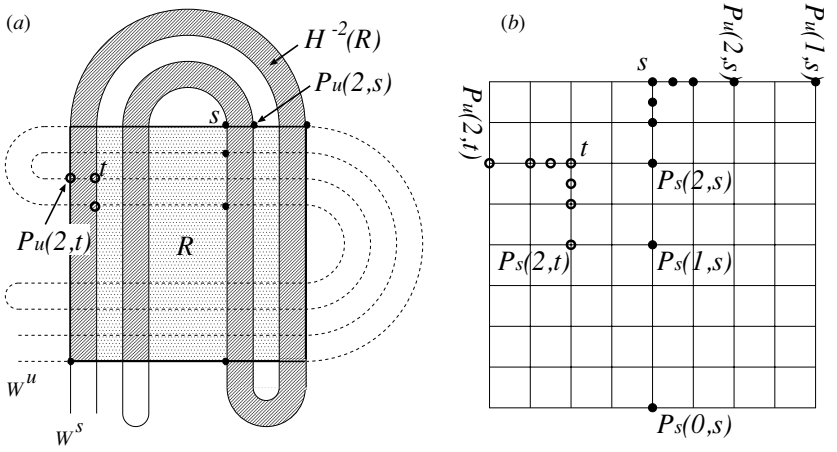

Figure 4. (*a*) Quadrilateral R and its backward image $H_a^{-2}(R)$. Both $\mathbf{s}$ and $P_u(2, \mathbf{s})$ are the endpoints of a segment of $H_a^{-2}(R) \cap W^u$. So are $\mathbf{t}$ and $P_u(2, \mathbf{t})$. (*b*) Sequences of P_u and P_s in the symbol plane for $\mathbf{s} = (0^\infty 1 \cdot 110^\infty)$ and $\mathbf{t} = (0^\infty 111 \cdot 0010^\infty)$. In the case of $\mathbf{s}$, $T_h = 1$ and $T_t = 0$. As for $\mathbf{t}$, since $T_h = T_t = 2$, $P_u(1, \mathbf{t})$, $P_s(0, \mathbf{t})$ and $P_s(1, \mathbf{t})$ are not defined (see (5)).

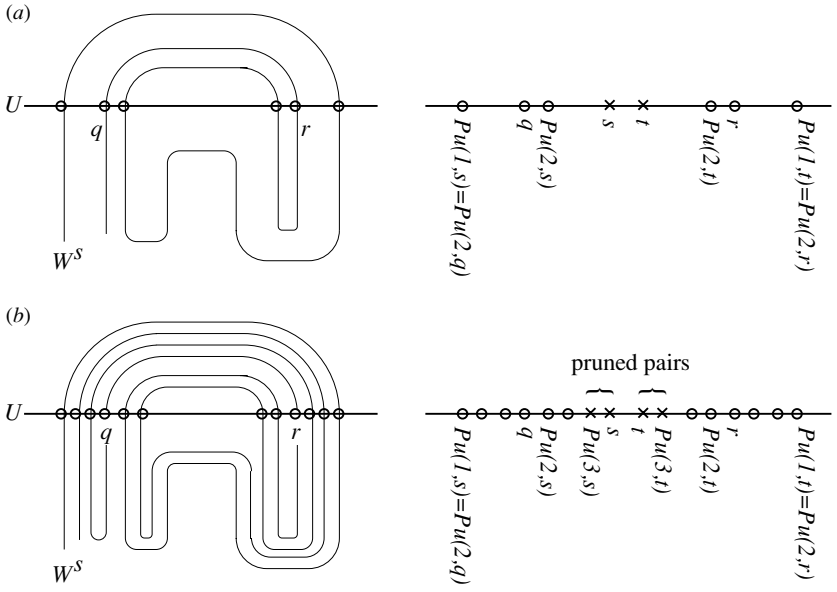

Figure 5. (*a*) Homoclinic points on U up to transition time 2 at a certain parameter value a after the horseshoe structure is destroyed. Here, the two points $\mathbf{s}$ and $\mathbf{t}$ have already disappeared. They do not have pruned pairs of length 2 and less. (*b*) Homoclinic points up to transition time 3 at the same a as (*a*). Now both $\mathbf{s}$ and $\mathbf{t}$ have pruned pairs of length 3. Circles and crosses stand for existing points and missing points, respectively.

If both $\mathbf{s}$ and $P_u(h, \mathbf{s})$ (resp. $P_s(t, \mathbf{s})$) are pruned at a certain a, we say that they are the *pruned pair of length* h (resp. t) on the unstable (resp. stable) manifold. We demonstrate this aspect in figure 5. Note that a pair of homoclinic points bifurcating with each other is *not* a pruned pair. The reason is given by the following propositions.

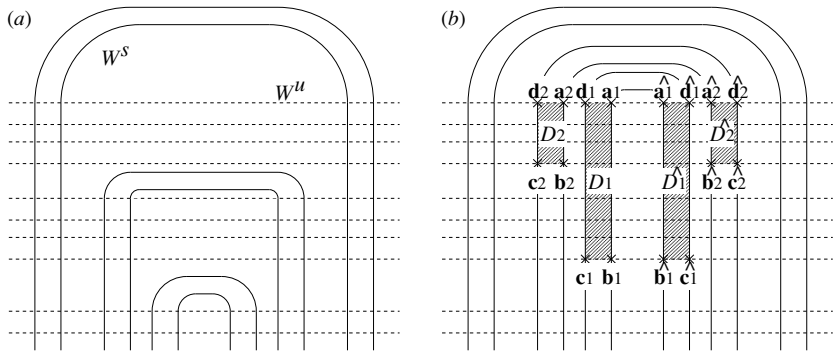

Figure 6. (*a*) Part of pruned horseshoe. (*b*) The corresponding pruned region drawn on the complete horseshoe. It is composed of the blocks D_1, $\hat{D}_1$, D_2 and $\hat{D}_2$, and their vertices are shown as crosses.

Proposition 1 (forcing relation [21])**.** *Before two homoclinic points* **s** *and* **t** *bifurcate, all homoclinic points in* $W^u[\mathbf{s}, \mathbf{t}] \cup W^s[\mathbf{s}, \mathbf{t}]$ *must have disappeared and the two must be neighbours on both* W^u *and* W^s*.*

Proposition 2 [21]**.** *If two homoclinic orbits bifurcate, their transition time must be equal. (Suppose that they are adjacent to each other on U. If their transition time is different, they are not adjacent to each other on S, which means that they cannot bifurcate.)*

By definition, **s** and $P_u(h, \mathbf{s})$ always have different transition times. Therefore by proposition 2, they never bifurcate with each other.

We say that a homoclinic point **s** undergoes a *primary bifurcation* if it bifurcates with $\hat{\mathbf{s}}$. The notation $\hat{\mathbf{s}}$ stands for the point symmetric to **s** with respect to the vertical centre line. That is, $\hat{\mathbf{s}} := (\ldots s_{-1} \cdot \hat{s_0} s_1 \ldots)$. If **s** and $\hat{\mathbf{s}}$ collide in a saddle-node bifurcation, it is a primary bifurcation. Suppose a pitchfork bifurcation occurs among three points **s**, $\hat{\mathbf{s}}$ and **t** at $a = a_1$ and the remaining point **t** collides with $\hat{\mathbf{t}}$ at $a = a_2$ as shown in figure 3. Then we consider that **s** and $\hat{\mathbf{s}}$ undergo a primary bifurcation at $a = a_1$, while **t** and $\hat{\mathbf{t}}$ do so at $a = a_2$.

3. A pruning algorithm

In this section we provide our pruning algorithm. The main stream is given in the next subsection, and the subroutines called in it are in the following two subsections.

3.1. Main routine

For a given parameter a at which the area-preserving Hénon map H_a is hyperbolic, the following algorithm gives the primary pruned region D for H_a. As shown in figure 6, D is given as a union of blocks denoted by D_j whose vertices are homoclinic points. Steps 2 and 3, which will be given below, provide the vertices of those blocks. Applying the continuation method, we judge whether or not a given homoclinic point is pruned, and make use of this information in the procedure. All homoclinic points which have undergone primary bifurcations at parameter values larger than a are contained in D.

1. Setting the initial conditions.
   1.1. Let the two homoclinic points on U undergoing the first bifurcation be $\mathbf{a}_1$ and $\hat{\mathbf{a}}_1$. That is, $\mathbf{a}_1 \leftarrow (0^\infty 1 \cdot 010^\infty)$ and $\hat{\mathbf{a}}_1 \leftarrow (0^\infty 1 \cdot 110^\infty)$, where arrows stand for substitution.
   1.2. Let the number of blocks j be 1.

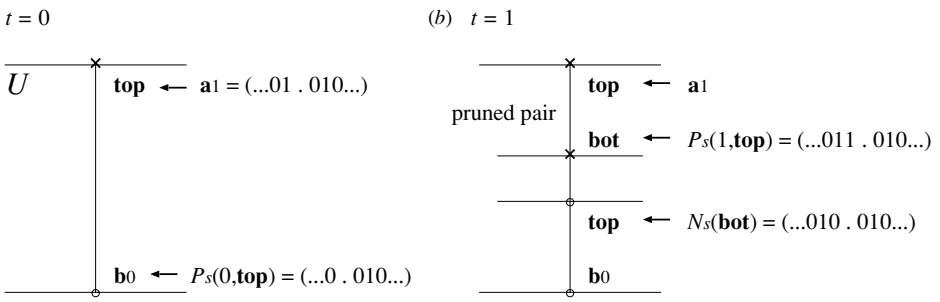

Figure 7. Example of the procedure to determine the depth of a block. (*a*) At $t = 0$, suppose that $\mathbf{top} = \mathbf{a}_1$ is missing and $P_s(0, \mathbf{top}) = \mathbf{b}_0$ is existing. So add 1 to t and start again from $\mathbf{a}_1$. (*b*) At $t = 1$, suppose further $P_s(1, \mathbf{top})$ is missing. So let $P_s(1, \mathbf{top})$ be **bot** and update **top** as $N_s(\mathbf{bot})$. If $N_s(\mathbf{bot})$ is an existing point as shown in the figure, we should choose this **bot** as $\mathbf{b}_1$ and finish the subroutine.

2. Finding the depth of the block D_j.
   Check whether or not homoclinic points are already pruned at a, starting from $\mathbf{a}_j$ and $\hat{\mathbf{a}}_j$, respectively, and scanning in the downward direction of the symbol plane. Here we apply the continuation method for this checking procedure. As presented in section 3.2, we can find the two points $\mathbf{b}_j$ and $\hat{\mathbf{b}}_j$ such that they have undergone a primary bifurcation and are the most distant points from $\mathbf{a}_j$ and $\hat{\mathbf{a}}_j$ (see figure 6).
3. Finding the width of the block D_j.
   Examine pruned homoclinic points similarly, starting from $\mathbf{b}_j$ and $\hat{\mathbf{b}}_j$, respectively, in the horizontal direction of the symbol plane. We again apply the continuation method. As a consequence, we can find the two points $\mathbf{c}_j$ and $\hat{\mathbf{c}}_j$ such that they have undergone a primary bifurcation. The details are given in section 3.3.
4. Let the rectangles three of whose vertices are given by $\mathbf{a}_j$, $\mathbf{b}_j$, $\mathbf{c}_j$ and $\hat{\mathbf{a}}_j$, $\hat{\mathbf{b}}_j$, $\hat{\mathbf{c}}_j$ be D_j and $\hat{D}_j$, respectively. That is,
$$D_j \leftarrow \{\mathbf{s} \in \Sigma_2 \mid (\mathbf{b}_j)_- \preceq \mathbf{s}_- \preceq (\mathbf{a}_j)_-, (\mathbf{c}_j)_+ \preceq \mathbf{s}_+ \preceq (\mathbf{b}_j)_+\}$$
$$\hat{D}_j \leftarrow \{\mathbf{s} \in \Sigma_2 \mid (\mathbf{b}_j)_- \preceq \mathbf{s}_- \preceq (\mathbf{a}_j)_-, (\hat{\mathbf{b}}_j)_+ \preceq \mathbf{s}_+ \preceq (\hat{\mathbf{c}}_j)_+\}.$$
   These blocks constitute the primary pruned region D.
5. The fourth vertex of D_j is given as $\mathbf{d}_j \leftarrow (0^\infty 1 \cdot (\mathbf{c}_j)_+)$.
   5.1. Let the left neighbour of $\mathbf{d}_j$ be $\mathbf{a}_{j+1}$, i.e. $\mathbf{a}_{j+1} \leftarrow N_u(\mathbf{d}_j)$.
   5.2. If both $\mathbf{a}_{j+1}$ and $\hat{\mathbf{a}}_{j+1}$ are missing, then add 1 to j and return to step 2.
   If either $\mathbf{a}_{j+1}$ or $\hat{\mathbf{a}}_{j+1}$ (or both) exist, then the loop terminates, because there are no more points undergoing primary bifurcations.
6. Let the union of all the blocks be D, i.e. $D \leftarrow \bigcup_{i=1}^{j}(D_i \cup \hat{D}_i)$. (END)

3.2. Subroutine 1

Subroutine 1 determines the depth of D_j. It is executed at step 2 of the main routine and determines $\mathbf{b}_j$ which is one of the vertices of D_j. Figures 7 and 8 will be helpful for the readers.

a. (Only when $j = 1$.)
   a.1. Set $t \leftarrow 0$, which is the initial condition for P_s.

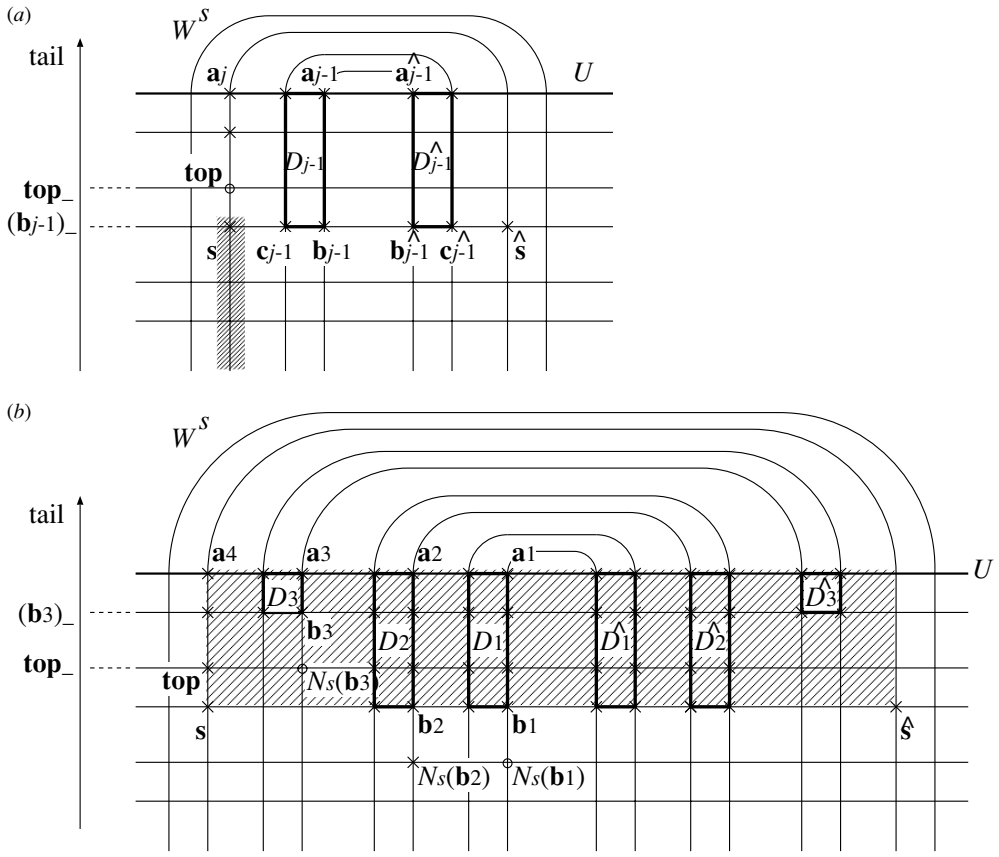

Figure 8. Illustration of step e of subroutine 1. (*a*) If **top** exists, the homoclinic points below **top** (shaded segment in the figure) do not undergo primary bifurcations. (*b*) If $\mathbf{top}_- \prec (\mathbf{b}_{j-1})_-$ (in this figure $j = 4$), at least one homoclinic point exists in the shaded area. Accordingly, in both cases the homoclinic points below **top** are not pruned by a primary bifurcation.

a.2. Set $\mathbf{b}_0 \leftarrow P_s(0, \mathbf{a}_1) = (0^\infty \cdot 010^\infty)$. This point is located at the bottom of the symbol plane and always exists. (If not, it implies that the fundamental segments are missing, because $H_a(\mathbf{b}_0) = q_u$ is one of the endpoints of S.)

b. Let $\mathbf{top} \leftarrow \mathbf{a}_j$. This is a missing point since we now assume the situation after the first tangency.

c. Find a pruned pair of **top** on the stable manifold.

c.1. If either $P_s(t, \mathbf{top})$ or $\hat{P}_s(t, \mathbf{top})$ exists, then add 1 to t and return to step b. By observation 3 mentioned in the next section, this loop terminates if the map H_a has hyperbolic structure.

c.2. Let $\mathbf{bot} \leftarrow P_s(t, \mathbf{top})$. These **bot** and **top** are the pruned pair of length t.

d. Let $\mathbf{top} \leftarrow N_s(\mathbf{bot})$.

e. If either **top** exists or $\mathbf{top}_- \prec (\mathbf{b}_{j-1})_-$, then the vertex is determined as $\mathbf{b}_j \leftarrow \mathbf{bot}$. Otherwise return to step c. (END)

The latest t is used as the initial value for constructing the next block D_{j+1}. The reason why the condition at step e terminates the routine is as follows.

First, suppose that a newly chosen **top** exists (see figure 8(*a*)), then no point in the shaded interval $\{\mathbf{s}|0^{\infty}\cdot \preceq \mathbf{s}_- \preceq \mathbf{top}_-, \mathbf{s}_+ = \mathbf{top}_+\}$ has undergone a primary bifurcation. This is because the existence of **top** on $W^s(\mathbf{s}, \hat{\mathbf{s}})$ contradicts proposition 1. As mentioned before, D is constructed so that it contains all the missing points which have undergone primary bifurcations. Therefore this interval need not be contained in D.

Second, suppose that the condition $\mathbf{top}_- \prec (\mathbf{b}_{j-1})_-$, which makes the sequence $(\mathbf{b}_1)_-, (\mathbf{b}_2)_-, \ldots$ increase monotonically, holds, and let the existing point having the largest subscript (i.e. the largest tail) among $N_s(\mathbf{b}_{j-1}), N_s(\mathbf{b}_{j-2}), \ldots, N_s(\mathbf{b}_1)$ be $N_s(\mathbf{b}_k)$. Then as shown in figure 8(*b*), in step e, **top** is chosen to satisfy $\mathbf{top}_- = (N_s(\mathbf{b}_k))_-$. Therefore if there is a missing point $\mathbf{s}$ below **top** on the vertical line including $\mathbf{a}_j$, the shaded area $\{\mathbf{t}|\mathbf{s}_- \preceq \mathbf{t}_- \preceq \mathbf{s}_-, \mathbf{s}_+ \preceq \mathbf{t}_+ \preceq \hat{\mathbf{s}}_+\}$ contains $N_s(\mathbf{b}_k)$. Thus by proposition 1, $\mathbf{s}$ is not pruned by a primary bifurcation.

3.3. Subroutine 2

Subroutine 2 determines the width of D_j. It is executed at step 3 of the main routine and determines $\mathbf{c}_j$ which is one of the vertices of D_j.

a. (Only when $j = 1$.)
   Set $h \leftarrow 2$, which is the initial condition for P_h. This makes $P_u(2, N_u P_u(2, \mathbf{b}_1))$ a point on the left border of the symbol plane.
b. Add 1 to h until either $P_u(h, N_u P_u(h, \mathbf{b}_j))$ or $P_u(h, \mathbf{b}_j)$ becomes a point pruned by a primary bifurcation.
c. Let the point determined at step b be $\mathbf{c}_j$. (END)

The latest h is used as the initial value for constructing the next block D_{j+1}. As shown in figure 9, for some h, $P_u(h, N_u P_u(h, \mathbf{b}_j))$ has undergone a primary bifurcation even though $P_u(h, \mathbf{b}_j)$ has not. Therefore, for each h, it is necessary to examine these two points as a candidate for $\mathbf{c}_j$.

When $\mathbf{c}_j$ is determined, it turns out that both $\mathbf{b}_j$ and $\mathbf{c}_j$ have the pruned pairs of length h on the unstable manifold. In particular, if $\mathbf{c}_j = P_u(h, \mathbf{b}_j)$, then $\mathbf{b}_j$ and $\mathbf{c}_j$ themselves are a pruned pair of each other. Due to hyperbolicity, this loop terminates within finitely many steps as well as the one in subroutine 1.

In the loops of the subroutines, with the increment of h (resp. t), the distance between homoclinic points $\mathbf{s}$ and $P_u(h, \mathbf{s})$ (resp. $P_s(t, \mathbf{s})$) is reduced in half. This loop is an example of procedures which pick up the vertices of blocks from infinitely many homoclinic points. One may find another procedure, for example, by which homoclinic points are examined equidistantly. So there exist several subroutines equivalent to ours.

4. Validity of the algorithm

In this section we first show that D constructed in this way satisfies the definition of a primary pruned region. Then we give the reason why our algorithm terminates within finitely many steps.

First, as a direct consequence of the procedure itself, the boundary of D is monotone and symmetric. Second, all orbits lying inside D are nonadmissible, because D_j is contained in the region encircled by $W^u[\mathbf{c}_j, \hat{\mathbf{c}}_j] \cup W^s[\mathbf{c}_j, \hat{\mathbf{c}}_j]$, which disappears when $\mathbf{c}_j$ and $\hat{\mathbf{c}}_j$ degenerate. Thus by proposition 1, all orbits lying on D_j also disappear before $\mathbf{c}_j$ and $\hat{\mathbf{c}}_j$ do. Finally, we show that all forbidden orbits lie on D. In order to prove this fact, assume that a homoclinic point $\mathbf{s}$ outside D is pruned. Let $\mathbf{s}'$ be a point bifurcating and disappearing with $\mathbf{s}$ according to our definition mentioned in section 2.2. Then both sequences differ in only one symbol,

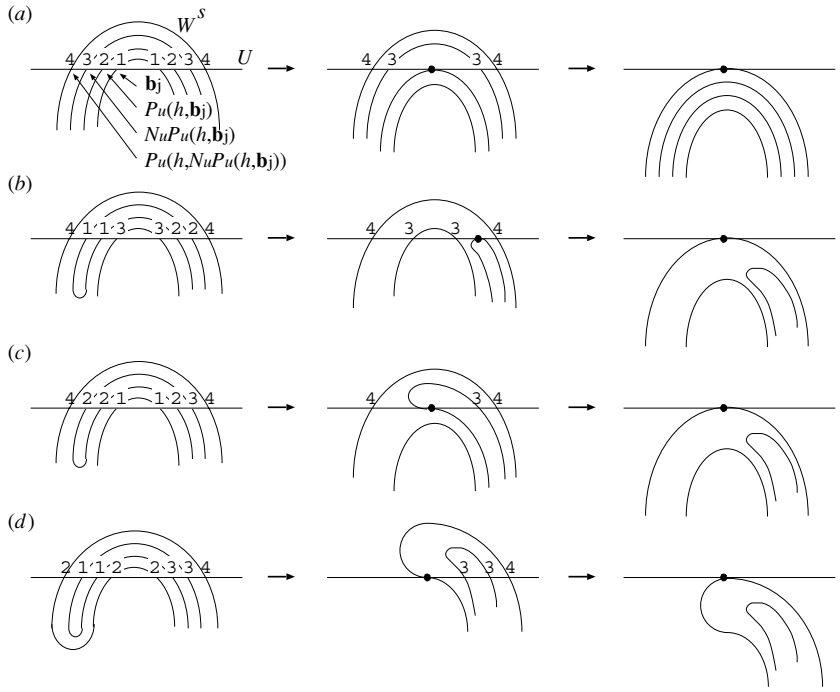

Figure 9. Examples of possible bifurcations. The numbers represent the order of bifurcations. In (*a*) and (*c*), $P_u(h, \mathbf{b}_j)$ undergoes a primary bifurcation. On the other hand, in (*b*) and (*d*), not $P_u(h, \mathbf{b}_j)$ but $P_u(h, N_u P_u(h, \mathbf{b}_j))$ does. Note that $P_u(h, \mathbf{b}_j)$ and $\hat{P}_u(h, \mathbf{b}_j)$ have different numbers.

because they are symmetric with respect to the line which separates either $W^u(\mathbf{s}, \mathbf{s}')$ or $W^s(\mathbf{s}, \mathbf{s}')$ just before the bifurcation. Iterate them so that the symbols next to the decimal point differ from each other. Then they are symmetric with respect to the vertical centre line. That is, these orbits have disappeared as a result of a primary bifurcation. Since D contains all missing points which have undergone primary bifurcations, we can say that the orbit of $\mathbf{s}$ lies on D.

Now we show the reason why the algorithm terminates within finitely many steps. The following observation is essential to this end.

Observation 3. *If the map H_a has neither tangential points between the stable and unstable manifolds nor points on U to which the stable manifold accumulates, then all pruned homoclinic points have pruned pairs of some length on both of the manifolds. In other words, for all pruned points $\mathbf{s}$, there exist h and t such that $P_u(h, \mathbf{s})$ and $P_s(t, \mathbf{s})$ are also pruned.*

We can make a similar statement on S. Here we explain why this observation is valid. For simplicity, let us consider pruned pairs on U. Suppose that on U there is a missing point which does not have any pruned pairs, i.e. a pruned point $\mathbf{s}$ such that $P_u(h, \mathbf{s})$ exists for all h.

As shown in figure 10(*a*), either the two points $\mathbf{s}_T$ and $\mathbf{t}_T$ or the others $\mathbf{q}_T := P_u(T, \mathbf{s}_T)$ and $\mathbf{r}_T := P_u(T, \mathbf{t}_T)$ have transition time T on U. Note that the tails of these four points are $0^\infty 1\cdot$. Let us assume that $\mathbf{s}_T$ and $\mathbf{t}_T$ collided with each other and disappeared as a decreased, and that neither $\mathbf{s}_T$ nor $\mathbf{t}_T$ has the pruned pair of length T, which is schematically shown in figure 10(*b*). Furthermore, suppose that they do not have pruned pairs of length less than T. When we consider the points up to transition time $T + 1$, a possible configuration is shown in

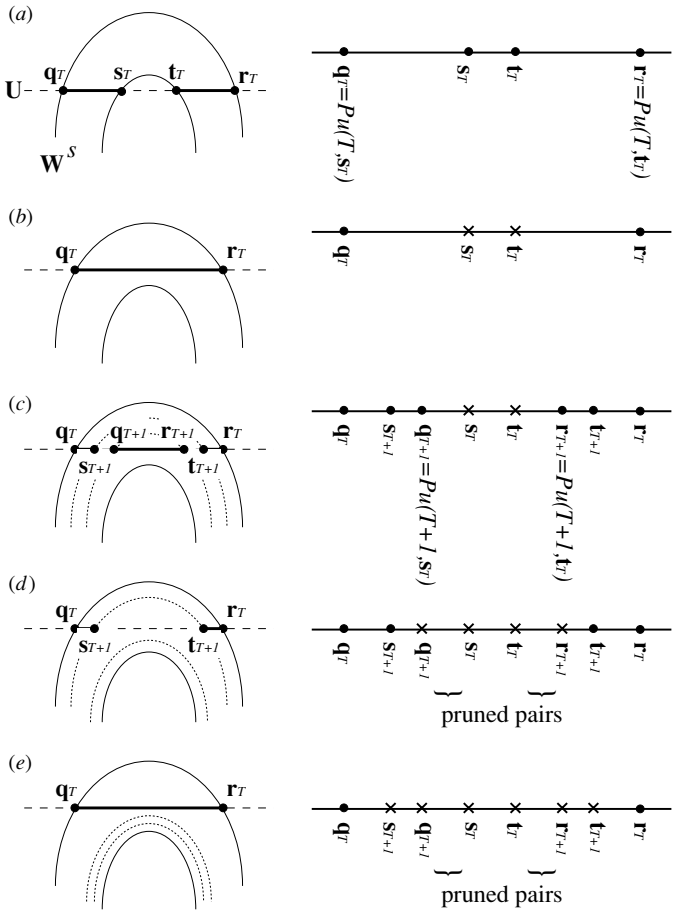

Figure 10. (*a*) Part of the manifolds at sufficiently large a. (*b*) Two points $\mathbf{s}_T$ and $\mathbf{t}_T$ in (*a*) disappear with decreasing a. (*c*), (*d*), (*e*) These are possible configurations when the points up to transition time $T+1$ are considered. In the cases of (*c*) and (*d*), there appear four and two new points, respectively. On the other hand, in the case of (*e*), there are no new homoclinic points in $W^u(\mathbf{q}_T, \mathbf{r}_T)$.

either figure 10(*c*), (*d*) or (*e*). However, if there is a missing point which does not have any pruned pairs on $W^u(\mathbf{q}_T, \mathbf{r}_T)$, either case (*c*) or (*e*) is the only one realizable. In the case of (*c*), new pruned points $\mathbf{q}_{T+1} := P_u(T+1, \mathbf{s}_T)$ and $\mathbf{r}_{T+1} := P_u(T+1, \mathbf{t}_T)$ are found. Thus $\mathbf{s}_T$ and $\mathbf{q}_{T+1}$ are the pruned pairs of length $T+1$. So are $\mathbf{t}_T$ and $\mathbf{r}_{T+1}$. However, at the same time two other pruned points $\mathbf{s}_{T+1} := N_u(\mathbf{q}_{T+1})$ and $\mathbf{t}_{T+1} := N_u(\mathbf{r}_{T+1})$ are also found; they do not have the pruned pairs of length $T+1$ and less. In the case of (*e*), the segment $W^u(\mathbf{q}_T, \mathbf{r}_T)$ is the same as that in (*b*).

In other words, no matter how large a transition time we consider, only either the case (*c*) or (*e*) is realizable. For any T, in $W^u(\mathbf{q}_T, \mathbf{r}_T)$, there are missing points which do not have the pruned pairs of length T and less. If the region encircled by $W^u(\mathbf{q}_\infty, \mathbf{r}_\infty) \cup W^s(\mathbf{q}_\infty, \mathbf{r}_\infty)$ has positive measure in the limit of $T \to \infty$, it contradicts the fact that there is no region in $\lim_{n\to\infty} H_a^{-n}(R)$ having a finite-length boundary and positive measure. Thus, the case (*c*) must be repeated infinitely many times; it implies that the length of $W^u(\mathbf{q}_T, \mathbf{r}_T)$ shrinks to

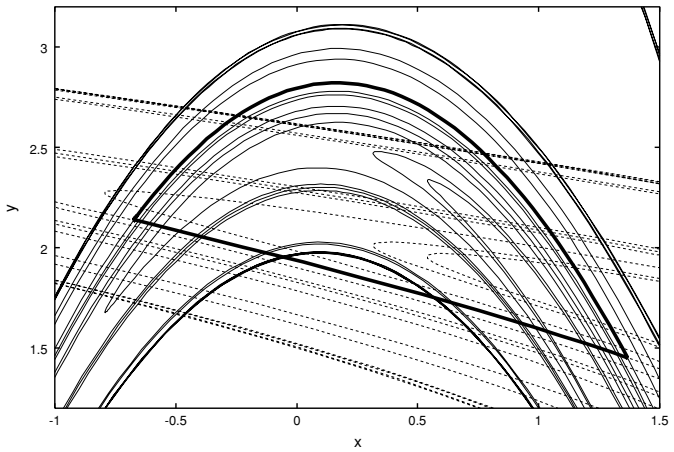

Figure 11. Part of the stable and unstable manifolds at $a = 4.58$.

zero. As a result, $\mathbf{q}_\infty$ and $\mathbf{r}_\infty$ must degenerate into either a tangential point or a point to which the stable manifold accumulates. This contradicts the assumption.

5. Examples

In this section, we trace our procedure to generate the primary pruned region D for a parameter interval including $a = 4.58$. Figures 11 and 12 show the stable and unstable manifolds at $a = 4.58$ and its schematic picture, respectively. The corresponding primary pruned region obtained via our algorithm is given as a union of blocks D_j and $\hat{D}_j$ in figure 12.

The first step of the main routine is to put $\mathbf{a}_1 = (0^\infty 1 \cdot 010^\infty)$. The depth of D_1 is determined in subroutine 1. Each step is taken in the following way (see figure 13). For $t = 0$, since the parameter value under consideration is one after the first tangency, $\mathbf{top} \leftarrow \mathbf{a}_1$ is missing (a cross in the figure). As step c, let $P_s(0, \mathbf{top}) = (0^\infty \cdot 010^\infty)$ be taken, and check whether it is pruned or not by applying the continuation method. In this case we find that it is an existing point (a circle in the figure). So letting $t = 1$, we find that $P_s(1, \mathbf{top}) = (0^\infty 11 \cdot 010^\infty)$ also exists. Then we move to the case $t = 2$. Both $P_s(2, \mathbf{top}) = (0^\infty 101 \cdot 010^\infty)$ and $\hat{P}_s(2, \mathbf{top})$ are missing, thus let **bot** be $P_s(2, \mathbf{top})$ and update **top** as $N_s(\mathbf{bot}) = (0^\infty 111 \cdot 010^\infty)$. Since the newly chosen **top** is missing and $\mathbf{top}_- = 0^\infty 111 \cdot \succ 0^\infty \cdot = (\mathbf{b}_0)_-$, the condition of step e is not satisfied. Therefore return to step c. Then taking $P_s(2, \mathbf{top}) = (0^\infty 11 \cdot 010^\infty)$, we find that this exists. So let $t = 3$ and start again from step b. In the same way, when $t = 5$ and $\mathbf{top} = (0^\infty 111 \cdot 010^\infty)$, both $P_s(5, \mathbf{top}) = (0^\infty 100111 \cdot 010^\infty)$ and $\hat{P}_s(5, \mathbf{top})$ are missing. So let **bot** be $P_s(5, \mathbf{top})$ and update **top** as $N_s(\mathbf{bot}) = (0^\infty 110111 \cdot 010^\infty)$. This time we find that **top** is an existing point, which means that the loop terminates. Consequently, $\mathbf{b}_1 \leftarrow \mathbf{bot} = (0^\infty 100111 \cdot 010^\infty)$ and $t = 5$ are the output of subroutine 1.

Now back to main routine, we next determine the width of D_1, which is done in subroutine 2. Examining from $P_u(1, \mathbf{b}_1)$ by employing the continuation method, we can find that $P_u(4, \mathbf{b}_1)$ has been pruned by a primary bifurcation. So let $\mathbf{c}_1$ be $P_u(4, \mathbf{b}_1) = (0^\infty 100111 \cdot 010010^\infty)$ and $h = 4$. Although infinitely many bifurcations occur in this

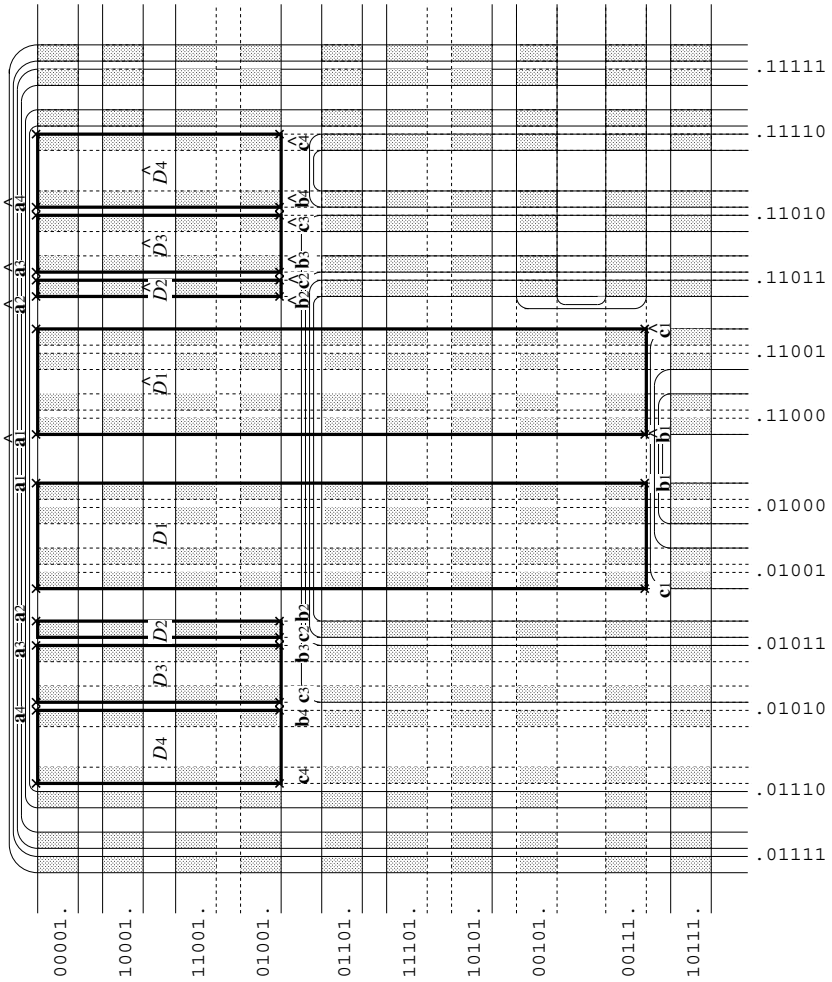

Figure 12. Schematic picture of the stable and unstable manifolds in the region encircled by a thick curve in figure 11. The solid lines show the manifolds, and the crosses stand for the vertices of the pruned blocks. The primary pruned region D is $\bigcup_{i=1}^{4}(D_i \cup \hat{D}_i)$. See also the last two diagrams in figure 16.

process, the crucial information is only a bifurcation diagram of $P_u(h, \mathbf{b}_1)$ $(h = 1, 2, \ldots)$, which is shown in figure 14. We then get the first two blocks D_1 and $\hat{D}_1$ as follows:

$$\begin{aligned} D_1 &= \{\mathbf{s} \mid (\mathbf{b}_1)_- \preceq \mathbf{s}_- \preceq (\mathbf{a}_1)_-, (\mathbf{c}_1)_+ \preceq \mathbf{s}_+ \preceq (\mathbf{b}_1)_+\} \\ &= \{\mathbf{s} \mid 0^\infty 100111\cdot \preceq \mathbf{s}_- \preceq 0^\infty 1\cdot, \cdot 010010^\infty \preceq \mathbf{s}_+ \preceq \cdot 010^\infty\} \\ &= \{01 \cdot 0100\} \cup \{00111 \cdot 0100\} \\ \hat{D}_1 &= \{01 \cdot 1100\} \cup \{00111 \cdot 1100\}. \end{aligned}$$

Because both $\mathbf{a}_2 = (0^\infty 1 \cdot 010110^\infty)$ and $\hat{\mathbf{a}}_2 = (0^\infty 1 \cdot 110110^\infty)$ are missing, we can construct the second two blocks D_2 and $\hat{D}_2$. Using $t = 5$ as the initial value, subroutine 1 yields the output $\mathbf{b}_2 = (0^\infty 1001 \cdot 010110^\infty)$, while it does not change t. As for the width,

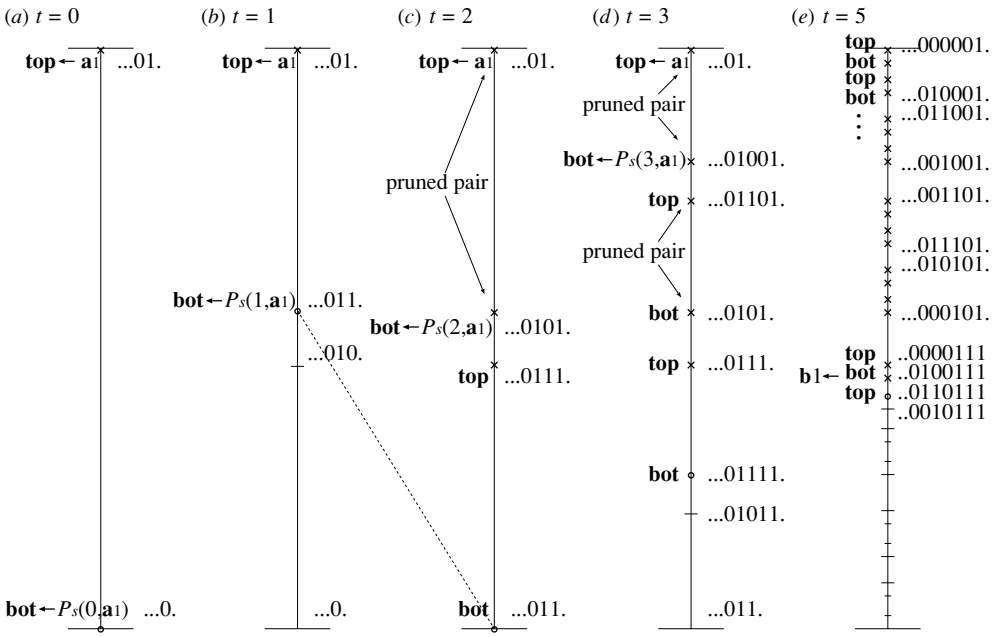

Figure 13. Procedure of subroutine 1 to obtain $\mathbf{b}_1$ at $a = 4.58$. All points in the figure have the same head $\cdot 010^\infty$. An explanation is given in the text.

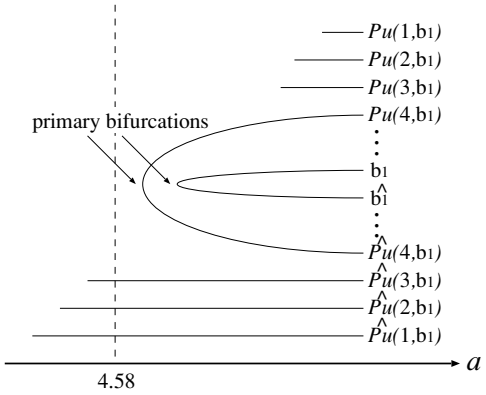

Figure 14. Schematic bifurcation diagram of $P_u(h, \mathbf{b}_1)$. This information suffices to decide $\mathbf{c}_1$, so we need not examine the entire stable and unstable manifolds. At the left endpoints of the straight line segments, the homoclinic orbits undergo saddle-node bifurcations with their partners, which are not shown in this figure.

using $h = 4$ as the initial value, subroutine 2 gives $\mathbf{c}_2 = (0^\infty 1001 \cdot 01011010^\infty)$ and $h = 6$. Hence,

$$\begin{aligned} D_2 &= \{\mathbf{s} \mid 0^\infty 1001\cdot \preceq \mathbf{s}_- \preceq 0^\infty 1\cdot, \cdot 01011010^\infty \preceq \mathbf{s}_+ \preceq \cdot 010110^\infty\} \\ &= \{001 \cdot 010110\} \\ \hat{D}_2 &= \{001 \cdot 110110\}. \end{aligned}$$

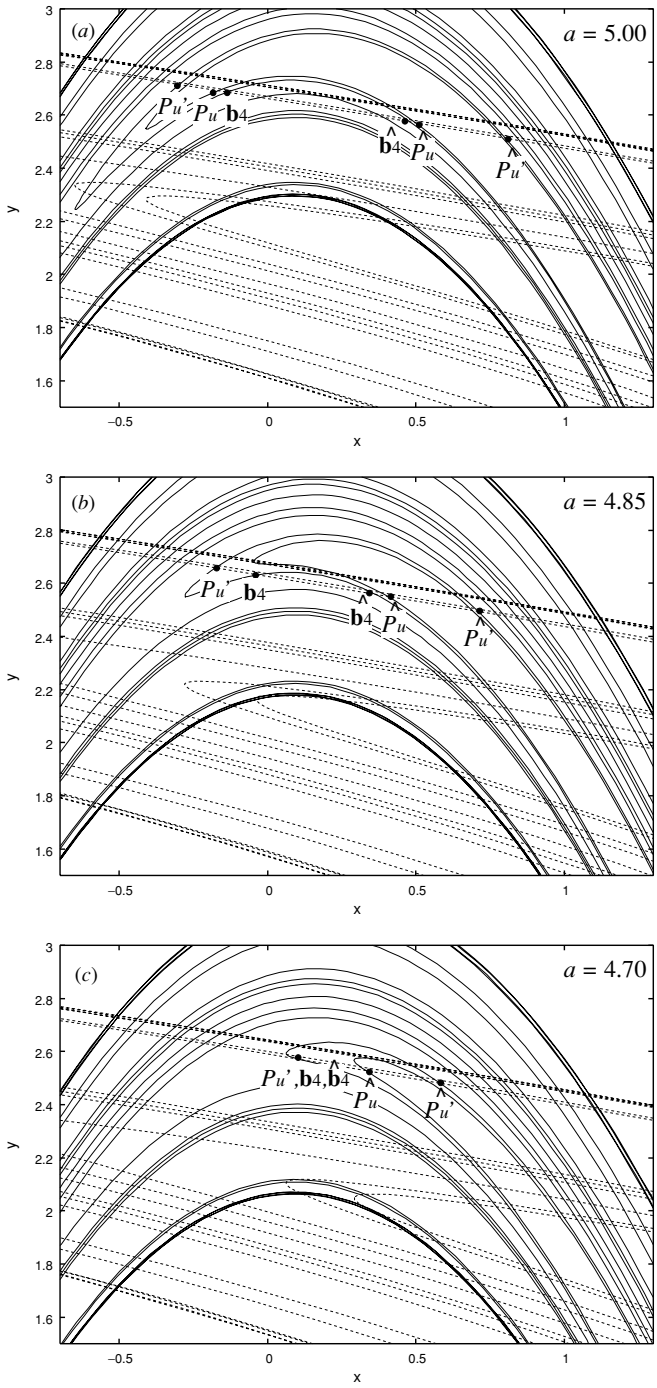

Figure 15. Stable and unstable manifolds at three parameter values larger than $a = 4.58$. In these figures, we use abbreviations P_u and P_u' for $P_u(6, \mathbf{c}_4)$ and $P_u(6, N_u P_u(6, \mathbf{c}_4))$, respectively. (*a*) All the related homoclinic points $\mathbf{b}_4$, $\hat{\mathbf{b}}_4$, P_u, $\hat{P}_u$, P_u' and $\hat{P}_u'$ are existing. (*b*) Although P_u has disappeared, $\hat{P}_u$ still exists, meaning that the type of bifurcation for P_u is not primary. (*c*) A pitchfork bifurcation takes place among three points P_u', $\mathbf{b}_4$ and $\hat{\mathbf{b}}_4$. By definition, the survivor is P_u'. Then P_u' and $\hat{P}_u'$ undergo a primary bifurcation.

Table 1. The endpoint parameter values [21] and the forbidden substrings for the same parameter intervals shown in figure 16. A symbol X denotes both 0 and 1.

Left endpoints	Right endpoints	Length of intervals	Forbidden substrings	
5.6319 ...	5.6776 ...	0.0457 ...	0001X1000	
5.5649 ...	5.6087 ...	0.0438 ...	0001X1001	001X1000
5.1885 ...	5.5376 ...	0.3491 ...	001X100	
4.8431 ...	4.8679 ...	0.0248 ...	001X10101	0001X101001
			10101X100	100101X1000
			001X1011	001X100
			1101X100	
4.5593 ...	4.5956 ...	0.0363 ...	001X11100	001X101
			00111X100	01X100

Moreover, the following four blocks can be constructed in the same way:

$$D_3 = \{001 \cdot 0101X1\} \qquad D_4 = \{001 \cdot 01X100\}$$
$$\hat{D}_3 = \{001 \cdot 1101X1\} \qquad \hat{D}_4 = \{001 \cdot 11X100\},$$

where $X = 0, 1$. Here both t and h remain unchanged when these blocks are obtained. It should be noted that $\mathbf{c}_3 = P_u(6, N_u P_u(6, \mathbf{b}_3)) = (0^\infty 1001 \cdot 01010110^\infty)$ and $\mathbf{c}_4 = P_u(6, N_u P_u(6, \mathbf{b}_4)) = (0^\infty 1001 \cdot 01110010^\infty)$. As for $\mathbf{c}_4$, note that $P_u(6, \mathbf{b}_4)$ has not pruned by a primary bifurcation. As shown in figure 15, some homoclinic points on $W^u(P_u(6, \mathbf{b}_4), \hat{P}_u(6, \mathbf{b}_4))$ such as $\mathbf{b}_4$ and $\hat{\mathbf{b}}_4$ survive even after $P_u(6, \mathbf{b}_4)$ disappeared. This just corresponds to the case given in figure 9(*d*). A similar argument can be applied to $\mathbf{c}_3$.

Finally, since both $\mathbf{a}_5 = (0^\infty 1 \cdot 01110110^\infty)$ and $\hat{\mathbf{a}}_5 = (0^\infty 1 \cdot 11110110^\infty)$ are existing, the main routine terminates here. Consequently, we obtained the primary pruned region $D = \bigcup_{i=1}^{4}(D_i \cup \hat{D}_i)$ which is shown in figure 12.

Figure 16 shows examples of the primary pruned regions for several parameter values. Near $a = 5.40$, the area-preserving Hénon map has the longest hyperbolic interval. We refer to the binary words representing a primary pruned region as the *forbidden substrings*. For the upper three intervals, the forbidden substrings coincide with what were obtained by Davis *et al* [14], who called them 'missing blocks'. Table 1 presents a list of forbidden substrings and the parameter values corresponding to the endpoints of the intervals calculated by Sterling *et al* [21].

6. Markov shifts and topological entropy

In the hyperbolic case, the primary pruned region is represented as a finite list of forbidden substrings. The dynamics of such a system is described by a Markov shift. In this section, we explain how to construct it.

Suppose that the length of the longest forbidden substrings is n. Then the Markov shift of a finite type is expressed as the transition between $n - 1$ symbols. That is,

$$\begin{aligned}
&\left(\ldots s_0 \cdot \boxed{s_1 \ldots s_{n-1}}\, s_n s_{n+1} s_{n+2} \ldots\right)\\
&\left(\ldots s_0 s_1 \cdot \boxed{s_2 \ldots s_n}\, s_{n+1} s_{n+2} \ldots\right)\\
&\left(\ldots s_0 s_1 s_2 \cdot \boxed{s_3 \ldots s_{n+1}}\, s_{n+2} \ldots\right)\\
&\qquad\vdots
\end{aligned}$$

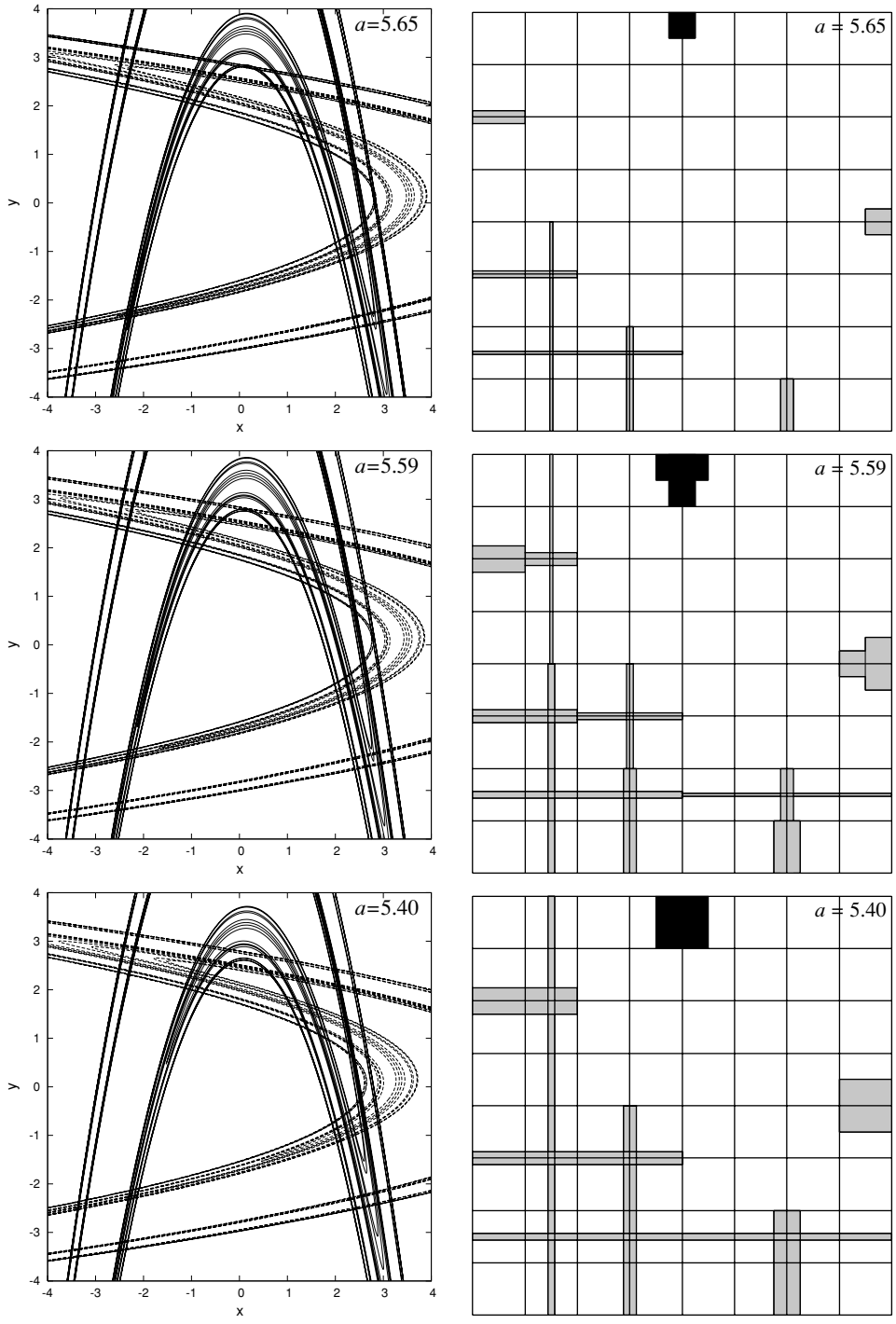

Figure 16. Stable and unstable manifolds and the pruned regions for the longest five intervals where the area-preserving Hénon map exhibits hyperbolic structure. The primary pruned regions are coloured black and their forward and backward images grey. The pruned regions for $a = 5.65$, $a = 5.59$ and $a = 5.40$ coincide with what Davis *et al* [14] obtained.

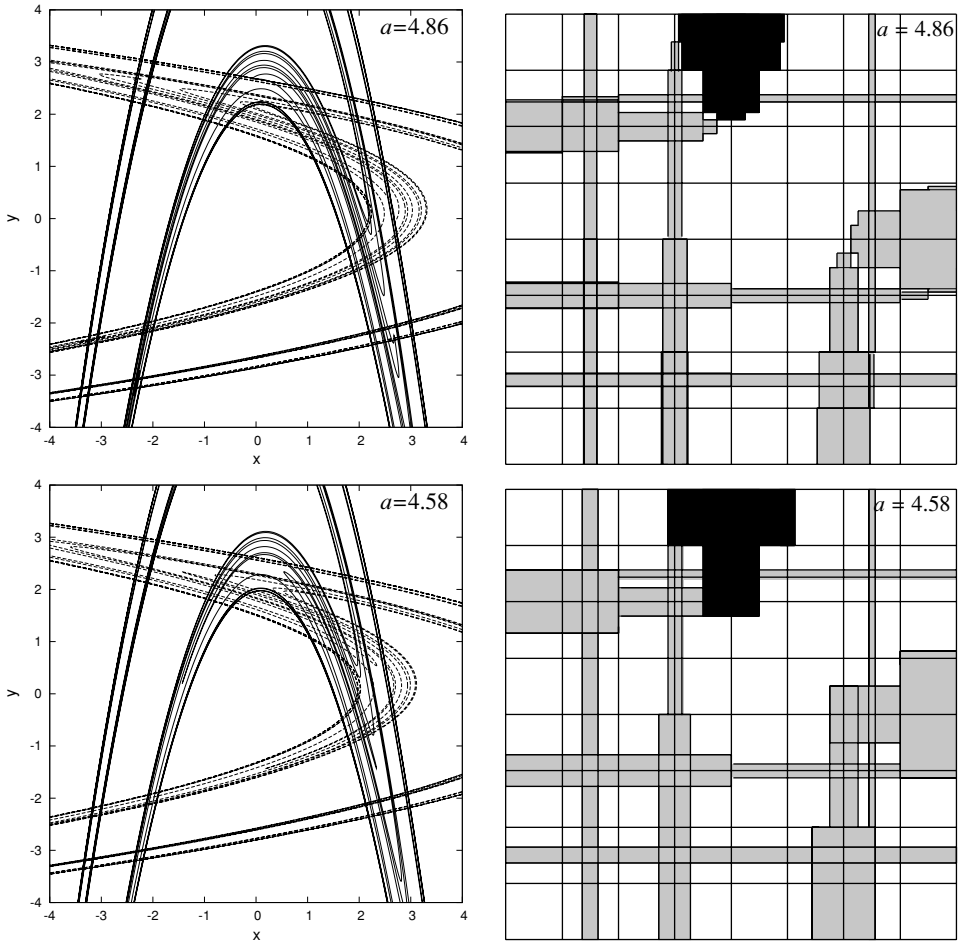

Figure 16. (Continued.)

$$
\begin{array}{c}
\\
000000 \\
001010 \\
001110 \\
\\
\\
\\
111111
\end{array}
\begin{array}{c}
\begin{array}{cccccc} 000000 & & 010100 & & 011100 & & 111111 \end{array} \\
\left(\begin{array}{cccccc}
1\ 1 & & \vdots & & \vdots & \\
 & \ddots & \vdots & & \vdots & \\
\cdots & \cdots & \mathbf{0}\ 1 & & \vdots & \\
 & & & \ddots & \vdots & \\
\cdots & \cdots & \cdots & \cdots & \mathbf{0}\ 1 & \\
 & & & & & \ddots \\
 & & & & & 1\ 1 \\
1\ 1 & & & & & \\
 & \ddots & & & & \\
 & & \ddots & & & \\
 & & & \ddots & & \\
 & & & & \ddots & \\
 & & & & & \ddots \\
 & & & & & 1\ 1
\end{array}\right)
\end{array}
\tag{6}
$$

For example, the forbidden substrings for $a = 5.40$, which is in the longest hyperbolic interval of the area-preserving Hénon map, are 0010100 and 0011100. Due to the absence of these

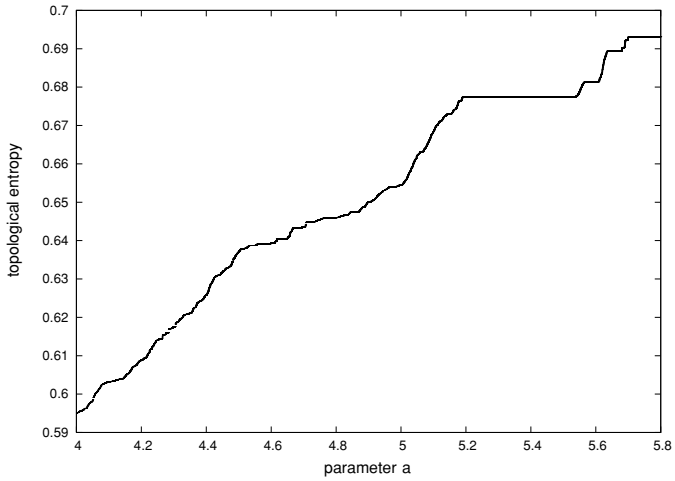

Figure 17. Topological entropy for the area-preserving Hénon map as a function of the parameter a. The resolution of the symbol plane, that is, the length of the forbidden substrings is fixed as 20.

substrings, the following two types of transitions are forbidden,

$$\ldots \cdot \boxed{0\,0\,1\,0\,1\,0}\,0\ldots \quad \longrightarrow \quad \ldots 0 \cdot \boxed{0\,1\,0\,1\,0\,0}\ldots$$
$$\ldots \cdot \boxed{0\,0\,1\,1\,1\,0}\,0\ldots \quad \longrightarrow \quad \ldots 0 \cdot \boxed{0\,1\,1\,1\,0\,0}\ldots.$$

Since each block is composed of six symbols, the Markov partition is obtained by dividing the nonwandering set into 2^6 pieces according to the symbol entries. The resulting structure matrix is a 2^6-dimensional one like (6), which has already been presented by some works [3, 4]. Every row in the matrix has at most two 1s in its entry, because a block overlaps the next one except for the last symbol. In general, if the length of the longest forbidden substrings is n, we have to prepare 2^{n-1}-dimensional structure matrix. The matrices are, though they have redundancy, automatically constructed once the primary pruned regions are obtained.

A structure matrix T gives the number of periodic points of the map σ:

$$\#(\text{fixed points of } \sigma^n) = \operatorname{tr} T^n \qquad (n \in \mathbb{N}). \tag{7}$$

For each parameter interval shown in figure 16, we confirmed that the numbers of periodic points calculated on the basis of structure matrices coincide with those calculated using the method proposed by Biham and Wenzel [29]. This justifies that what we obtained are proper Markov partitions.

As an additional application, we calculate the topological entropy for the area-preserving Hénon map as a function of the parameter a in figure 17. The topological entropy is obtained as the logarithm of the maximal eigenvalue of the structure matrix.

We limit the maximal length of forbidden strings to 20 and ignore the finer structures of the primary pruned regions. For non-hyperbolic parameter values, we cope with approximate structure matrices, because our algorithm may not terminate and does not give precise pruned regions.

Above $a = 5.699\ldots$ at which the first tangency occurs [21], symbolic dynamics forms the binary full shift, and the topological entropy is equal to log 2. As shown in figure 17, the entropy decreases monotonically with the parameter from the first tangency point. Although the plot well resembles that of the number of periodic orbits [14], we should remark that monotonicity

is just a result of the assumption of no bubbles, and that our algorithm necessarily yields a monotonic increase in the pruned region.

Collins presented a method to estimate lower bounds of the topological entropy of planar diffeomorphisms with homoclinic tangles [30]. Our results coincide with those calculated using the method of Collins for the hyperbolic parameter intervals shown in figure 16. Even in the case of non-hyperbolic parameter intervals, we observed that the entropy computed with our algorithm seems to converge, as we increase the resolution of the symbol plane. However, there is no guarantee that it gives either a lower or an upper bound of the entropy.

7. Conclusion and discussion

In this paper, we have presented an automatic algorithm to obtain the primary pruned region for the area-preserving Hénon map. Our prescription makes full use of a bifurcation diagram of homoclinic orbits on the fundamental segments of the stable (or unstable) manifold. It is obtained by applying the continuation of orbits from the anti-integrable limit.

Hyperbolicity of the map, which is a crucial assumption for actual construction, ensures the procedure terminates within finitely many steps. For a non-hyperbolic system, meaning that the map presents homoclinic tangencies for example, the algorithm will not construct the exact pruned regions. Even in such a case, we can obtain some blocks and can tell that at least these blocks are pruned.

Since the idea of pruning was proposed, the monotonicity and symmetry of the pruning front have always been a matter of discussion. The possibility of anti-monotonic [6] and asymmetric [12] pruning fronts was mentioned. In this paper, they are consequences of the construction. However, if two homoclinic orbits with different transition times bifurcate and disappear, in other words, if there occur bifurcations, which are not assumed in proposition 2, then our algorithm may not work. This implies the existence of asymmetric pruning fronts, the importance of which was discussed in [12].

All the combinatrices arising from bifurcations are contained in a bifurcation diagram in advance. Therefore, what we have done is just converting information of homoclinic orbits on a one-dimensional fundamental segment to that in the two-dimensional symbol plane, in which the pruning front is drawn. However, since we have only to check the existence or non-existence of homoclinic orbits on a fundamental segment, our algorithm is straightforward and easily implemented. As stressed in the introduction, our present attempt is not to construct the generating partition, for which several prescriptions have been proposed so far [2, 10, 15–19]. What we have done in this paper is just to draw the pruning front in the symbol plane, not to draw the border in the configurational (x, y) plane.

A primary pruned region allows one to construct the Markov partition and the structure matrix related to it. As an immediate outcome of the Markov partition, we have evaluated the topological entropy of the map. All these are consistent with the preceding results.

Finally, we mention a further application of the proposed algorithm. The topological entropy may certainly be an important invariant quantity for dynamical systems, but it does not specify all the topological characters. For example, as indicated in the previous section, our transition matrices have much redundancy. In other words, the Markov partition thus obtained is not a unique partition, but there are infinitely many other possibilities. So we may naturally ask to what extent we can reduce the number of partitions, that is, the minimum number of the partitions, which would provide different topological characterization of a dynamical system. This question is almost equivalent to asking the minimum number of states of the automaton which generates symbol sequences of a given map, and also the *grammatical complexity* introduced in the context of the formal language [31]. The grammatical complexity for the

Hénon and the Lozi maps is also indeed computed systematically as a function of the system parameter in our subsequent paper [32].

Acknowledgments

The authors would like to thank Y Ishii and A Sannami for their stimulating discussions and valuable comments.

References

[1] Milnor J and Thurston W 1988 On iterated maps of the interval *Dynamical Systems (College Park, MD, 1986–7)* (Berlin: Springer) pp 465–563
[2] Wang Q and Young L-S 2001 Strange attractors with one direction of instability *Commun. Math. Phys.* **218** 1–97
[3] Cvitanović P, Gunaratne G and Procaccia I 1988 Topological and metric properties of Hénon type strange attractors *Phys. Rev.* A **38** 1503–20
[4] Cvitanović P 1991 Periodic orbits as the skeleton of classical and quantum chaos *Physica* D **51** 138–51
[5] Hansen K T 1993 Symbolic dynamics: I. Finite dispersive billiards *Nonlinearity* **6** 753–69
[6] Ishii Y 1997 Towards a kneading theory for Lozi mappings I: a solution of the pruning front conjecture and the first tangency problem *Nonlinearity* **10** 731–47
[7] Lozi R 1978 Un attracteur étrange(?) du type attracteur de Hénon *J. Phys. (Paris)* **39** *Colloq.* C5 9–10
[8] Hénon M 1976 A two-dimensional mapping with a strange attractor *Commun. Math. Phys.* **50** 69–77
[9] Friedland S and Milnor J 1989 Dynamical properties of plane polynomial automorphisms *Ergodic Theor. Dyn. Syst.* **9** 67–99
[10] Sannami A 2003 Nonexistence of symbolic representation for discrete dynamical systems *Preprint*
[11] de Carvalho A 1999 Pruning fronts and the formation of horseshoes *Ergodic Theor. Dyn. Syst.* **19** 851–94
[12] de Carvalho A and Hall T 2002 How to prune a horseshoe *Nonlinearity* **15** R19–68
[13] Hall T Prune Software available from *Nonlinearity* at stacks.iop.org/Non/15/R19 and http://www.liv.ac.uk/~tobyhall/prune
[14] Davis M J, MacKay R S and Sannami A 1991 Markov shifts in the Hénon family *Physica* D **52** 171–8
[15] Grassberger P and Kantz H 1985 Generating partitions for the dissipative Hénon map *Phys. Lett.* A **113** 235–8
[16] Grassberger P, Kantz H and Moenig U 1989 On the symbolic dynamics of the Hénon map *J. Phys. A: Math. Gen.* **22** 5217–30
[17] D'Alessandro G, Grassberger P, Isola S and Politi A 1990 On the topology of the Hénon map *J. Phys. A: Math. Gen.* **23** 5285–94
[18] Giovannini F and Politi A 1992 Generating partitions in Hénon-type maps *Phys. Lett.* A **161** 332–6
[19] Jaeger L and Kantz H 1997 Structure of generating partitions for two-dimensional maps *J. Phys. A: Math. Gen.* **30** L567–76
[20] Sterling D 1999 Anti-integrable continuation and the destruction of chaos *PhD Thesis* University of Colorado
[21] Sterling D, Dullin H R and Meiss J D 1999 Homoclinic bifurcations for the Hénon map *Physica* D **134** 153–84
[22] Dullin H R, Meiss J D and Sterling D 2000 Generic twistless bifurcations *Nonlinearity* **13** 203–24
[23] Kan I, Koçak H and Yorke J A 1992 Antimonotonicity: concurrent creation and annihilation of periodic orbits *Ann. Math.* **136** 219–52
[24] Devaney R and Nitecki Z 1979 Shift automorphisms in the Hénon mapping *Commun. Math. Phys.* **67** 137–46
[25] Sterling D and Meiss J D 1998 Computing periodic orbits using the anti-integrable limit *Phys. Lett.* A **241** 46–52
[26] Bedford E and Smillie J 2001 Real polynomial diffeomorphisms with maximal entropy: tangencies *Preprint* math.Ds/0103038
[27] Devaney R 1989 *An Introduction to Chaotic Dynamical Systems* 2nd edn (Redwood City, CA: Addison-Wesley)
[28] Easton R W 1986 Trellises formed by stable and unstable manifolds in the plane *Trans. Am. Math. Soc.* **294** 719–32
[29] Biham O and Wenzel W 1989 Characterization of unstable periodic orbits in chaotic attractors and repellers *Phys. Rev. Lett.* **63** 819–22
[30] Collins P 2002 Symbolic dynamics from homoclinic tangles *Int. J. Bifur. Chaos Appl. Sci. Eng.* **12** 605–17
[31] Wolfram S 1984 Computation theory of cellular automata *Commun. Math. Phys.* **96** 15–57
[32] Hagiwara R and Shudo A 2004 Grammatical complexity for two-dimensional maps *J. Phys. A: Math. Gen.* **37** 10545–59